Nuclear Instruments and Methods in Physics Research A 1064 (2024) 169410

Contents lists available at ScienceDirect

Nuclear Inst. and Methods in Physics Research, A

journal homepage: www.elsevier.com/locate/nima

Full Length Article

Design of the RF waveguide network for the klystron-based CLIC main linac RF module

P. Wang *, M. Capstick, N. Catalan Lasheras, S. Doebert, A. Grudiev, C. Rossi, P. Morales Sanchez, I. Syratchev, X. Wu

SY, CERN, Esplanade des Particules 1, Geneva, 1211, Geneva 23, Switzerland

ARTICLE INFO

Keywords:
CLIC
RF module
Accelerating structure
RF pulse compressor

ABSTRACT

The klystron-based Compact Linear Collider (CLIC) was initially proposed with a low center-of-mass energy of 380 GeV, primarily due to potential cost-effectiveness. To enhance overall cost-efficiency, reliability, and stability, a novel RF module for klystron-based CLIC main linac has been designed and studied. This RF module utilizes two X-band klystrons to feed eight traveling wave accelerating structures, resulting in a beam energy increase of 138 MeV. A key innovation of the new RF module is the integration of double-height waveguides, which contributes to a 30% reduction in surface fields and a 40% decrease in RF loss. To meet the double-height requirement, a majority of the RF components responsible for transmitting the high RF power underwent a redesign. Two solutions, based on the choke mode flange and the L-shape waveguide, were proposed to facilitate the adjustment of the accelerating structures for beam-based alignment. Additionally, bent damping waveguides and HOM loads and a high order Magic-T, were designed for the accelerating structure named CLIC-K. The paper will comprehensively present and describe both the RF design and the integration of the klystron-based CLIC module.

1. Introduction

The Compact Linear Collider (CLIC) is a linear electron-positron collider with center-of-mass energies of 380 GeV, 1.5 TeV and 3 TeV, as well as high luminosity [1–3]. Employing the Two-Beam acceleration scheme, CLIC sources its RF power feeding the main accelerating structures from the high-current driven beam [3]. This acceleration scheme has the advantage of cost-effectiveness for the TeV scale energies. However, its cost efficiency decreased significantly when addressing the lower center of mass of 380 GeV. Consequently, there is a contemplation on the adoption of a Klystron-based CLIC for the initial stage with an energy of 380 GeV [1,2]. The klystron-based scheme presents itself as a financially viable option, while beyond this energy threshold, the Two-Beam scheme emerges as the sole feasible alternative.

In the two-beam scheme, the high-current driven beam traverses Power Extraction and Transfer Structures (PETs), generating RF power for the accelerating structures [4,5]. The proximity between PETs and accelerating structures is a mere half meter, rendering the RF loss in the RF network negligible. The RF power generated by the PETs amounts to approximately 132 MW, maintaining a surface electric field in the RF network of only 33 MV/m [4]. In contrast, the klystron-based scheme introduces a distance of about 4 meters between the klystrons and accelerating structures, necessitating more RF components then the two-beam scheme for the RF power transmission, thereby incurring significant RF loss in the RF network. The RF power from two klystrons is combined, transported and then split into eight accelerating structures, with a pulse compression system increasing the peak RF power to 350 MW. However, this amplification results in substantially larger surface fields compared to the two-beam scheme. To mitigate RF loss and surface fields in the klystron-based scheme, RF components with double the height of the standard WR-90 waveguide have been proposed and investigated. Efforts have been made to maximize the use of these double-height RF components, as their incorporation is pivotal for ensuring the reliability and stability of the RF network.

Traditional standing wave or traveling wave structures do not require wakefield damping due to low beam current and a less stringent beam quality requirement [6–10]. However, in the case of CLIC, wakefield damping becomes a fundamental necessity [11,12]. Numerous traveling wave accelerating structures have been designed, fabricated and tested for the CLIC project [13–16]. An accelerating structure named CLIC-K, featuring straight damping waveguides, was specifically designed and studied for the klystron-based scheme. CLIC-K comprises two RF couplers and 26 regular cells [17]. Each cell incorporates four damping waveguides with Higher Order Mode (HOM) loads to

* Corresponding author.
E-mail address: ping.wang@cern.ch (P. Wang).

https://doi.org/10.1016/j.nima.2024.169410
Received 4 March 2024; Received in revised form 28 April 2024; Accepted 28 April 2024
Available online 30 April 2024

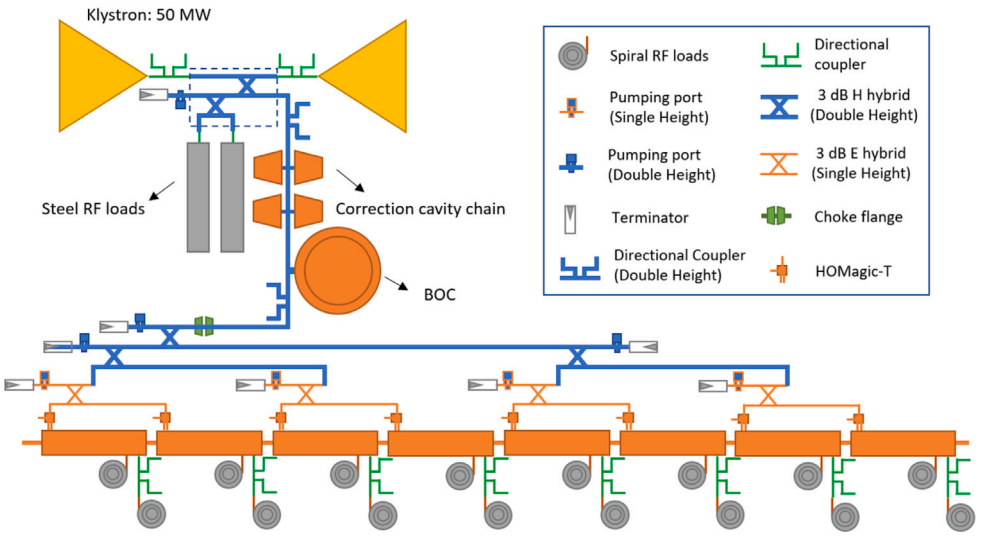

Fig. 1. Schematic layout of the RF module for klystron-based CLIC.

effectively absorb the wakefields generated by the electron beams traverse CLIC-K. For enhanced integration and a more compact design, we proposed the use of bent damping waveguides. Additionally, a High Order Mode Magic-T (HOMagic-T) was employed to damp wakefields originating from the input coupler [13]. A compact H-bend was designed to transmit the working mode at 12 GHz and the wakefield at 17 GHz for the accelerating structure.

The RF pulse compressor constitutes a critical component within the RF network for numerous linac-based projects [18–24]. A novel pulse compression system, incorporating a storage cavity and correction cavities, has been designed and investigated for the klystron-based scheme [25,26]. This system comprises an X-band SLAC Energy Doubler (SLED) type pulse compressor as the storage cavity and a correction cavity chain based on spherical cavities. Currently in use at CERN's Xbox2 high power test stand, the pulse compression system demonstrates excellent RF performance. However, its power gain of 3.5 is not large enough for the klystron-based scheme when considering the RF loss of the RF network [27]. To enhance power gain, a bowl cavity with an unloaded quality factor of 24.4e4 was studied for both the storage cavity and correction cavities [28]. A bowl cavity for the storage cavity is undergoing fabrication by Shanghai Advanced Research Institute in China. Finally, the pulse compression system based on a new Barrel Open Cavity (BOC) pulse compressor as the storage cavity and bowl cavities as the correction cavities has been designed and chosen as an ultimate solution for klystron-based CLIC [29].

The alignment specifications for the klystron-based scheme differ from the two-beam case. Beam-based alignment (BBA) has been proposed for CLIC [30]. A dedicated RF component is essential to facilitate the adjustment of the accelerating structures for BBA. To fulfill the BBA requirement, we propose two schemes that employ Choke Mode Flange (CMF) and L-shape waveguide (LSW), respectively.

Numerous RF components have been designed and employed in the high power X-band test facilities at CERN, as documented in [31]. The insights gained from this extensive experience prove invaluable in designing the RF module for klystron-based CLIC. Building upon this foundation, we have refined the RF components, introducing reduced tolerance requirements and enhancing RF parameters for improved performance.

The structure of the paper is outlined briefly below. In Section 2, we provide a schematic layout of the RF module along with the introduction of three kinds of RF loads proposed for the RF module. Section 3 covers a detailed description of the CLIC-K structure and the pulse compression system. Moving forward, Section 4 delves into the presentation of the RF combiner located between the klystrons and the pulse compression system, while Section 5 addresses the RF splitter located between the pulse compression system and the CLIC-K structures. The paper concludes with a summary in the final section.

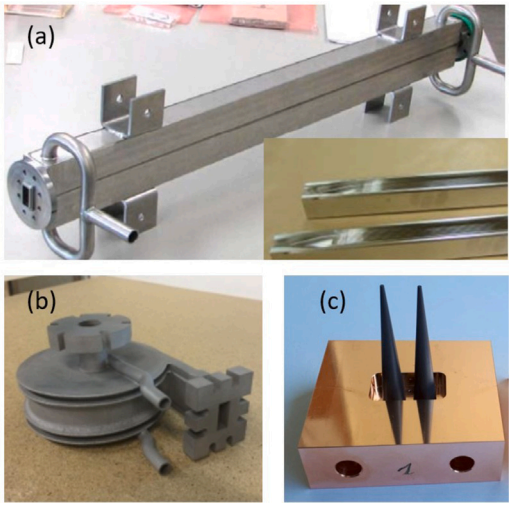

Fig. 2. Three RF loads for the RF module, (a) steel RF load, (b) spiral load and (c) RF terminator.

2. Schematic layout of RF module

Fig. 1 depicts the schematic layout of the RF designed for the klystron-based CLIC. To support a center-of-mass energy of 380 GeV, a total of 2754 such RF modules will be required. Each RF module comprises two klystrons with a peak power of 50 MW, a pulse compression system increasing the peak power by a factor of 3.80, and eight accelerating structures with an average loaded accelerating gradient of 75 MV/m. The installation of these eight accelerating structures on a girder necessitates precise alignment prior to the final integration. For the active BBA, it is imperative that the girder supporting the eight accelerating structures be movable. To facilitate this requirement, the CMF positioned between the pulse compression system and the power splitters is designed to allow movement without impacting RF power transmission. Another method involves using an LSW with bending, which also allows movement of the accelerating structures.

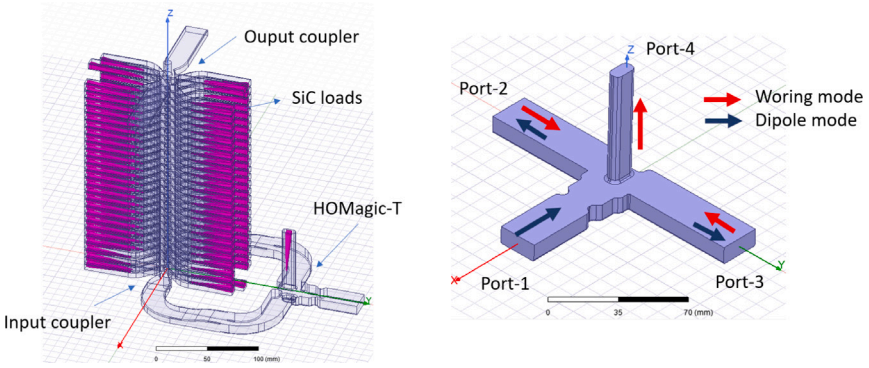

Fig. 3. CLIC-K structure based on smart disks with SiC loads and HOMagic-T.

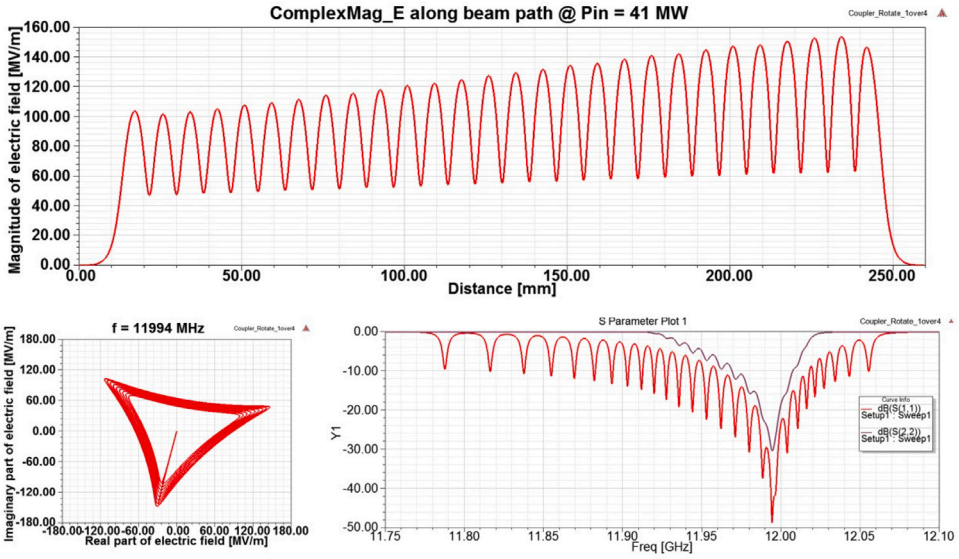

Fig. 4. Field distribution and s-parameters of CLIC-K structure.

In accordance with the RF power levels, the RF module can be categorized into five sections: the RF combiner, the double height waveguide (DHWR-90) with a length of 2 m, the pulse compression system, the RF splitter and the accelerating structure section. The RF combiner combines the RF power from two klystrons, generating a total RF power of 95 MW. Subsequently, The RF power transverses the DHWR-90 and reaches to the pulse compression system. The pulse compression system compresses the RF pulse, yielding a shorter RF pulse with a power of 350 MW. The RF splitter divides the RF power from the pulse compression system into four parts for distribution to the accelerating structure section. The accelerating structure section comprises four super accelerating structures (SAS), with each SAS featuring an E-plane 3-dB hybrid and two CLIC-K accelerating structures.

In this configuration, the CMF serves as an illustrative example. Positioned just after the pulse compression system, a single CMF satisfies the requirement for the BBA. In contrast to the CMF case, the accelerating structure section employs four LSWs, each corresponding to one SAS.

The RF module incorporates three types of RF loads: steel RF loads, spiral RF loads, and RF terminators, as shown in Fig. 2. The steel RF load is adapted to managing RF power exceeding 50 MW and finds application in the RF combiner section, where two steel RF loads can efficiently absorb the entire RF power from two klystrons. The compact spiral RF load is employed in the accelerating structure section, absorbing the RF power leaving the accelerating structures. The RF terminator is tasked with terminating the RF ports of the 3-dB hybrids in both the RF combiner and the RF splitter sections. Typically, only three ports of a 3-dB hybrid are utilized for transporting high RF power, leaving the fourth port with negligible RF power. Consequently, the utilization of the steel RF load and spiral RF loads becomes unnecessary under these ports. The RF terminator, characterized by its compact nature, facilitates the integration of the RF module. These ports are also used to integrate the vacuum pumping port just before the RF terminator.

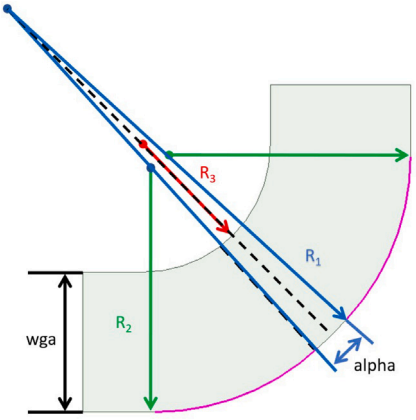

Fig. 5. RF model and main parameters of the bending waveguide.

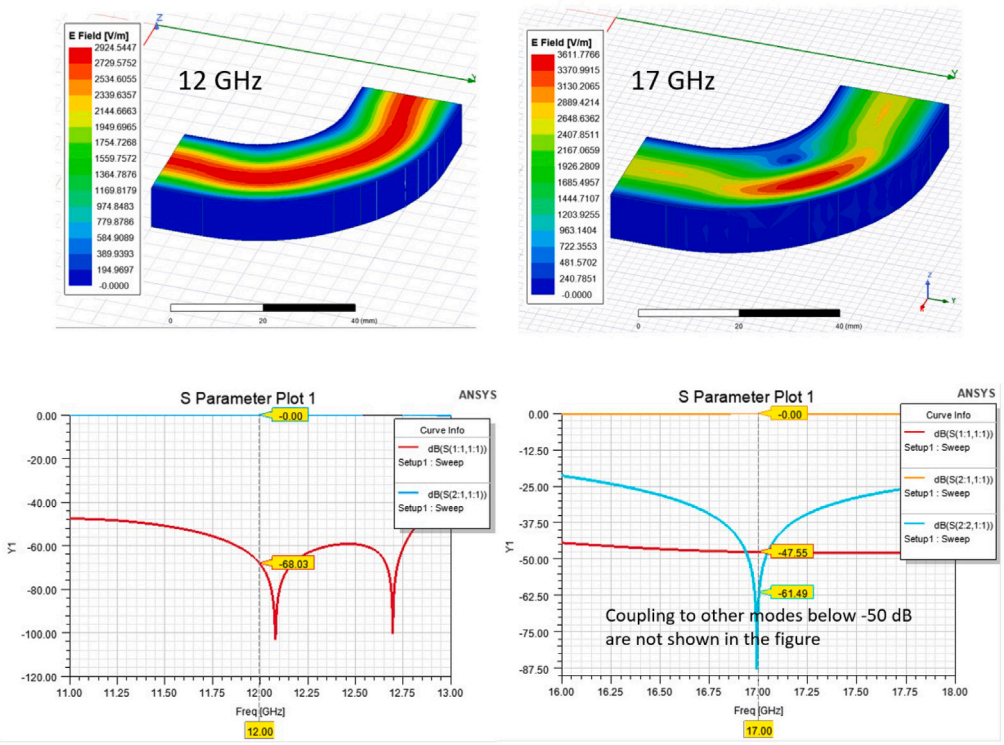

Fig. 6. Field distribution and S-parameters of the bending waveguide for 12 GHz and 17 GHz.

Each of these RF loads underwent thorough study and testing at the high-power test stand at CERN [32].

3. Accelerating structure and pulse compression system

The accelerating structures and pulse compression system serve as pivotal components within the RF module. All other RF components are designed in sequence after the development of these foundational elements.

The accelerating structure designated as CLIC-K, featuring straight damping waveguides, was specifically designed for klystron-based CLIC [17]. Initially, rounding disks were proposed for CLIC-K, followed by a detailed study and comparison with square disks with bent damping waveguides. Square disks proved superior in terms of compactness and ease of machining. The updated CLIC-K design incorporates the use of square disks, as shown in Fig. 3. CLIC-K comprises 2 RF couplers and 26 regular cells and has a length of 233 mm. Each regular cell integrates 4 bent damping waveguides with small HOM loads inside. The HOM loads made of SiC lossy material serve to absorb the wakefield generated by the beams traversing the cell. For the input coupler, two damping waveguides in the y direction handle wakefield damping in that direction, while an HOMagic-T is introduced to address wakefield damping in the x direction [13]. Unlike the traditional Magic-T, the waveguide on the H-plane has a small cross section, preventing the working mode with a frequency of 12 GHz and allowing the transmission of the dipole mode with a main frequency of 17 GHz. The dipole mode of the wakefield in the x direction of the input coupler is combined by the HOMagic-T and directed into the small waveguide, where an HOM load absorbs the wakefield. For more details on the principle for the HOMagic-T, see [13]. For the working mode with a frequency of 12 GHz, the HOMagic-T functions as an RF splitter.

The results of the RF design of the CLIC-K are shown in Fig. 4, mirroring those of the CLIC-K based on straight damping waveguides [17]. Inclusion of bent damping waveguides does not alter the RF parameters of the CLIC-K for the working mode. Specifically, the average loaded gradient of CLIC-K remains at 75 MV/m with an input power of 40.6 MW, and the phase advance of CLIC-K is 120 degrees. For additional details, see [17].

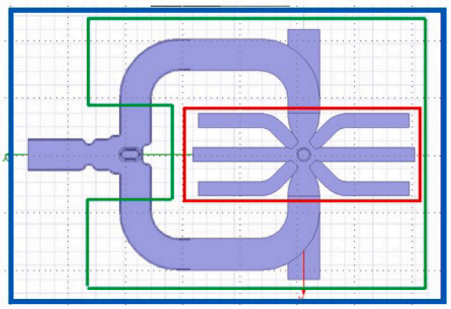

Fig. 7. RF model with three scenarios for wakefield calculation. Red zone: Perfect matching layer (PML) on the input coupler and loads in the dampling waveguides (PIC-LDw); Green zone: Shorted bends on the matching layer (PML) on the input coupler and loads in the dampling waveguides (SFIC-LDw); Blue zone: HOMagic-T on the input coupler and loads in the dampling waveguides (MTIC-LDw).

To achieve a comprehensive RF design characterized by compactness, the inclusion of a compact bending waveguide is imperative. Another crucial requirement is that both the working mode with a frequency of 12 GHz and the wakefield with a frequency of 17 GHz must exhibit favorable transmission properties in the bending waveguides. A dedicated bending waveguide was designed to meet these dual requirements, as shown in Fig. 5. The distinctive feature of this bending waveguide lies in the shape of the outer wall, which incorporates two arcs with radii denoted R1 and R3, respectively. The bending waveguide demonstrates excellent performance, with reflections below −47 dB, as shown in Fig. 6. Notably, the bending waveguide matches the performance of the straight waveguide at 12 GHz in terms of the passband and surface fields.

As mentioned above, the HOMagic-T serves the purpose of absorbing the wakefield from the input RF coupler in the x direction. To

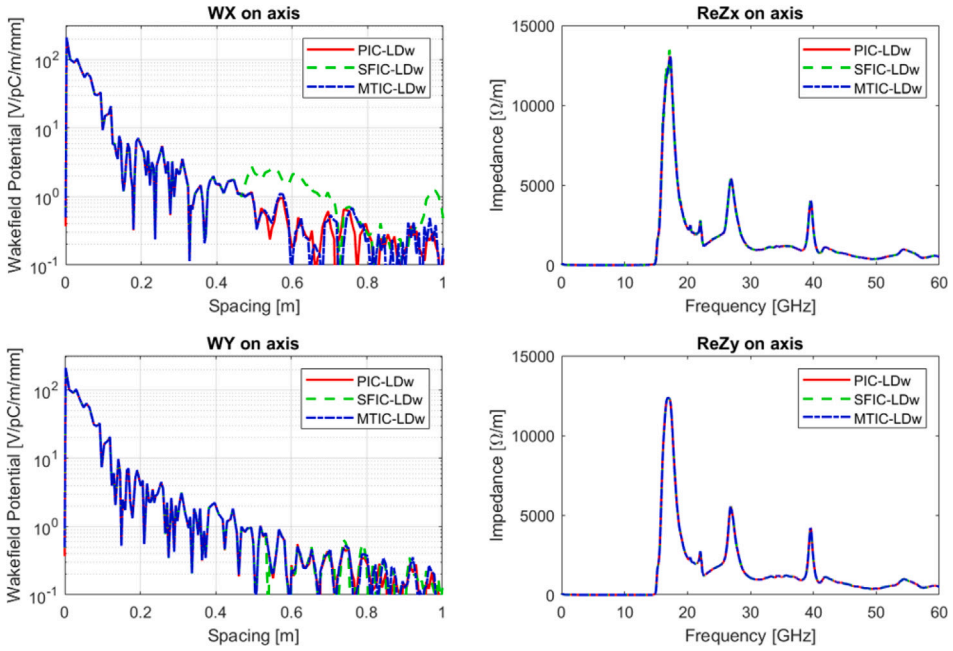

Fig. 8. Results of the wakefield simulation for three scenarios.

Table 1
F parameters in x direction for three scenarios.

Input coupler settings	Fc	Frms	Fworst
PIC-LDw-x	1.0021	1.1623	3.0745
SFIC-LDw-x	1.00444	1.2392	**64.37**
MTIC-LDw-x	1.0011	1.0692	2.2577
Limit	–	< 2	< 5

evaluate the necessity of the HOMagic-T, three cases were examined, as shown in Fig. 7. These cases are defined within three zones: the blue zone encompassed all RF components for the wakefield simulation, the green zone excludes the HOMagic-T, allowing the wakefield to be reflected by the short faces of the bending waveguides, and the red zone excludes both the bending waveguides and HOMagic-T. The results of these cases are shown in Fig. 8. Calculating the so-called jitter amplification parameters from the wakefields provides insights into the wakefield impact on the transverse beam stability [33]. The matrix A is used to calculate the jitter amplification parameters. The element of the matrix A is defined: $A_{jk} = \frac{(ia_1)^{(j-k)}}{(j-k)!}$, where j and k denote the bunch j and bunch k, i is imaginary number, and a_1 is calculated by using the wakefield. For more details on the matrix A, see [33]. Based on the matrix A, the three jitter amplification parameters are defined as follows: $F_c = \frac{1}{n}\sum_k \left|\sum_j A_{kj}\right|^2$ and $F_{rms} = \frac{\sum_{k=0}^{n-1}\sum_{j=1}^{k} A_{k,j}A_{k,j}^*}{n}$, where n is the number of bunches. The worst combination can be found via a singular value analysis of A. The square of the largest singular value then defines F_{worst}. The blue zone exhibits a wakefield reflection from the short faces, leading to unacceptable F parameters. In contrast, the other two cases show similar wakefields with acceptable F parameters, as listed in Table 1. Consequently, on the basis of these findings, the HOMagic-T is deemed essential for the optimal performance of the accelerating structure.

The pulse compression system for klystron-based CLIC is based on individual cavities. The input and output waveforms of the pulse compression system is shown in Fig. 9. A Barrel Open Cavity (BOC) pulse compressor and a correction cavity chain (CCC) utilizing bowl cavities were designed and studied, as shown in Figs. 10 and 11. The mode of the BOC pulse compressor is $TM_{1,1,32}$ which boasts an impressive unloaded quality factor of 23.5e4 and low surface fields.

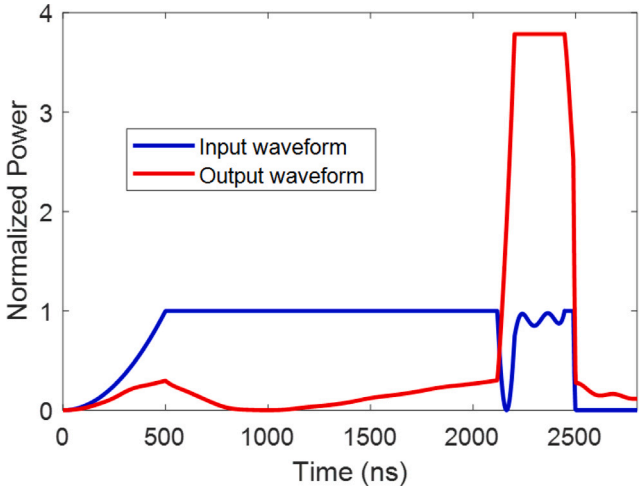

Fig. 9. Input and output waveforms of the pulse compression system.

The optimized coupling factor is 6.6 for the BOC pulse compressor. The bowl cavity uses a $TE_{2,2,3}$ mode and exhibits a unique feature of no field present at the top of the cavity, facilitating effective vacuum pumping. The unloaded quality factor is 7.5e4 and the optimized coupling factor is 1.95. For a more comprehensive understanding of the pulse compression system, please refer to [29].

4. RF combiner

The RF combiner, shown in Fig. 12, comprises 4 RF tapers, a pumping port, a double-height 3-dB hybrid and a splitter. It combines the RF power from two klystrons by using a 3-dB hybrid. The RF design and the S parameters of the 3-dB hybrid are shown in Fig. 13. A standard height of 10.16 mm was adopted for the RF design. The 3-dB hybrid, characterized by its compactness, exhibits a substantial pass band of 180 MHz, as defined by the merit function surpassing −30 dB. The merit function, denoted as:

$$db(1 - 2 * |ReS13 * ImS14 + ImS13 * ReS14|),$$

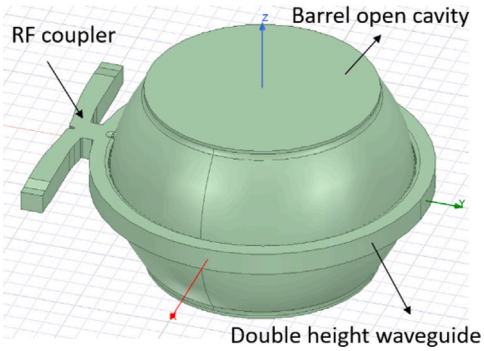

Fig. 10. RF model of the BOC pulse compressor.

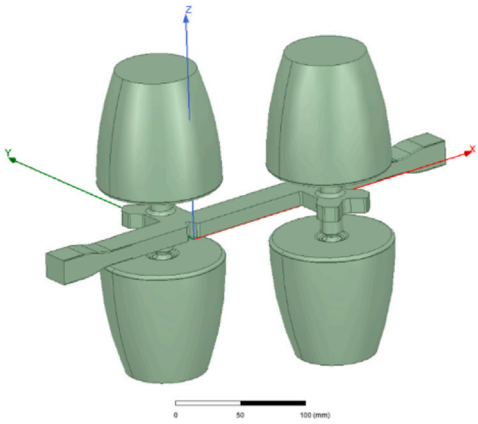

Fig. 11. RF model of the correction cavity chain based on bowl cavities.

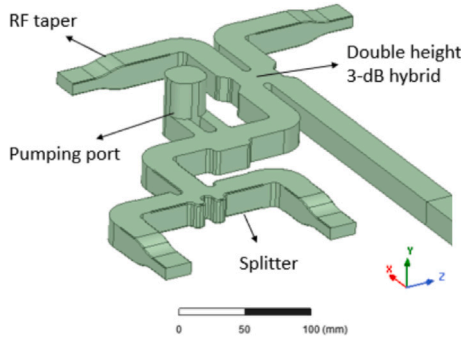

Fig. 12. RF combiner of the RF module for klystron-based CLIC.

is elaborated further in [34]. This H-plane device features symmetry based on an electric wall. A double height 3-dB hybrid can be achieved by doubling its height. The H-bends and pumping port of the RF combiner, also H-plane devices, can be adapted similarly to double-height versions simply by changing the height.

The output waveguides of the klystrons adhere to standard dimensions, with a height of 10.16 mm and a width of 22.86 mm. To establish a connection between these standard waveguides and double-height waveguides, an RF taper is employed. The RF design and the S parameters of the RF taper are shown in Fig. 14. Notably, the double-height waveguide can theoretically support four modes at a frequency of 12 GHz. Among these, the first mode corresponds to the working mode (TE10 mode). The couplings from working mode to the remaining three modes are below -60 dB, rendering them negligible. Additionally, the RF taper facilitates connection to the two steel RF loads.

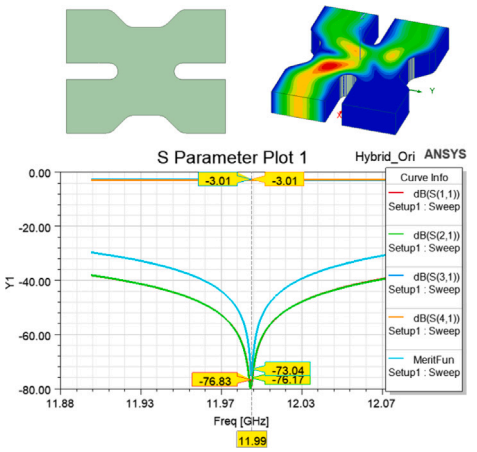

Fig. 13. RF design and s-parameters of the 3-dB hybrid.

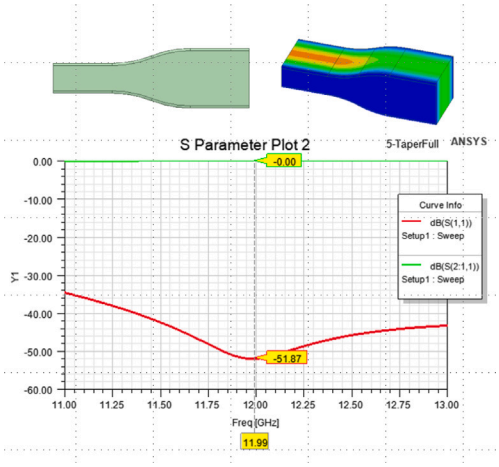

Fig. 14. RF design and S-parameters of the RF taper.

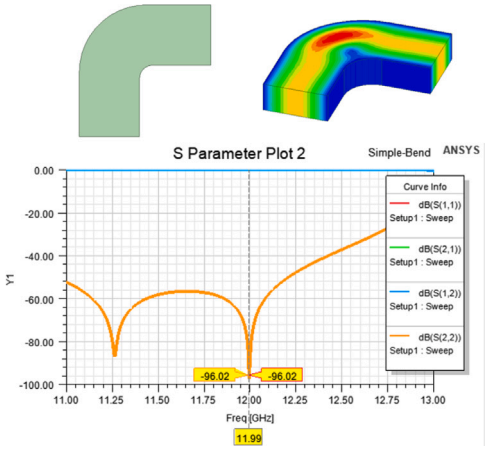

Fig. 15. RF design and S-parameters of the H-bend.

There are six H-bands in the RF combiner. The RF design and S-parameters of the H-band are shown in Fig. 15. The pass band, defined by the reflection better than -30 dB, exceeds 1 GHz. An additional advantage is that the tolerances for the geometric parameters exceed 0.1 mm, which facilitates fabrication.

A pumping port is incorporated into the RF combiner, as shown in Fig. 16. The pumping port can be considered as a 4-port device with

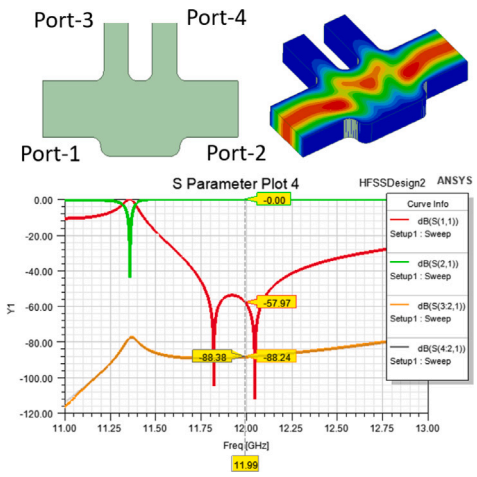

Fig. 16. RF design and S-parameters of the Pumping port.

effective isolation between port-1 and port-3, as well as between port-1 and port-4, both registering below −80 dB. Following the pumping port, an RF splitter is employed to distribute the RF power to two steel RF loads. The RF splitter has been thoroughly studied and tested at CERN [31].

5. RF splitting network

Following the pulse compression system, the RF power undergoes a two-fold division to feed four SASs. Two schemes have been proposed for the RF splitter. The first involves two double-height E-bends, a CMF, and three double-height 3-dB hybrids, as shown in Fig. 17. The second scheme comprises a double-height E-bend, three double-height 3-dB hybrids, and four LSWs, as shown in Fig. 18.

The double-height E-bend is a E-plane device without symmetry based on the electric wall, distinguishing it from the cases of double-height H-band, pumping port and 3-dB hybrid. The RF design and the S parameters are shown in Fig. 19. For the simulation, four modes are considered for each port. The reflection of the working mode and couplings to the other modes are consistently below −50 dB.

The CMF and LSW are designed to facilitate the movement of the accelerating structure section, meeting the requirements of BBA. The RF design of the CMF is shown in Fig. 20. The CMF comprises rectangular waveguide parts, rectangular waveguide adapters to the circular waveguide, circular waveguides, and a choke. The CMF is bifurcated by the choke, allowing relative movement of the two parts for adjustments of the position of the accelerating structure section. The S parameters of the CMF in the normal case are shown in Fig. 21. The transmission of the working mode from port-1 to port-2 is nearly 100%. With a transmission better than 99.99%, acceptable offset ranges of the three directions can be calculated. For the x-direction, the range is ±0.89 mm; for the y-direction, the range is ±0.12 mm; and for the z-direction, the range is ±0.96 mm. In the RF splitter, adjustments in the y direction and the z direction are selected for movement. The LSW features L-shaped waveguides with a length of 0.5 m for each arm, allowing similar adjustment ranges for the x-direction and z-direction. The LSW waveguides are standard waveguides with a height of 10.16 mm. The advantage of the LSW-based scheme is that no special mechanical design is needed for the LSW to control movement. However, the disadvantage is that the RF loss is greater than that of the CMF-based scheme.

6. Mechanical design and integration

Based on the RF components mentioned above, two mechanical design integration layouts were developed, as shown in Figs. 22 and 23 [35]. These layouts incorporate considerations for the tunnel in klystron-based CLIC, vacuum maintenance, and other integration considerations for the RF module. Real positions of the RF components

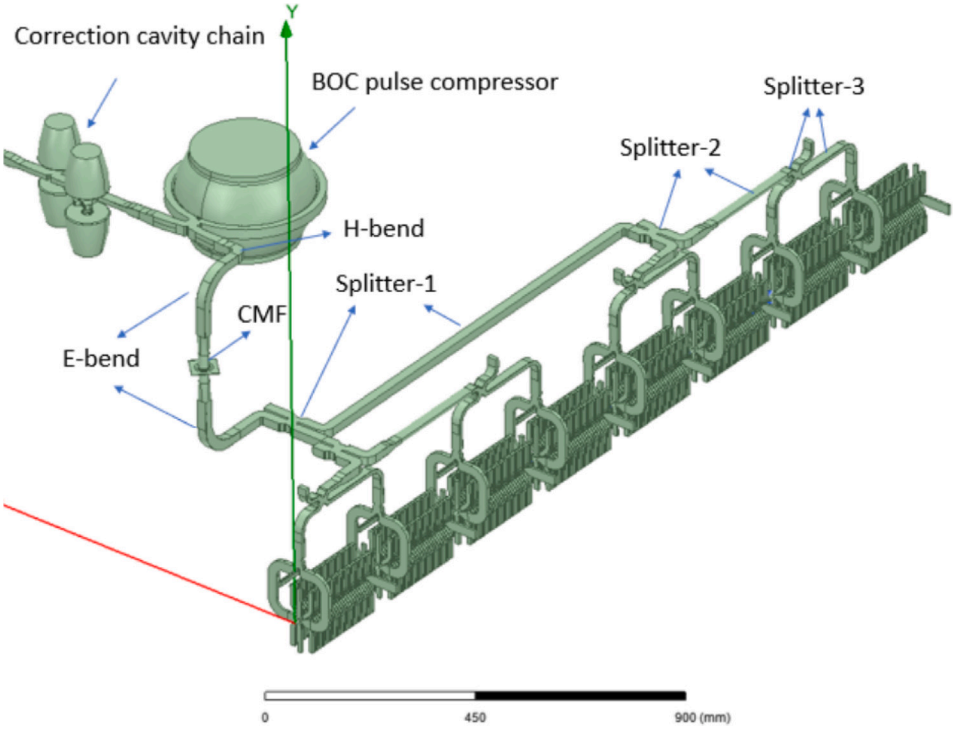

Fig. 17. RF design of the RF splitter based on CMF.

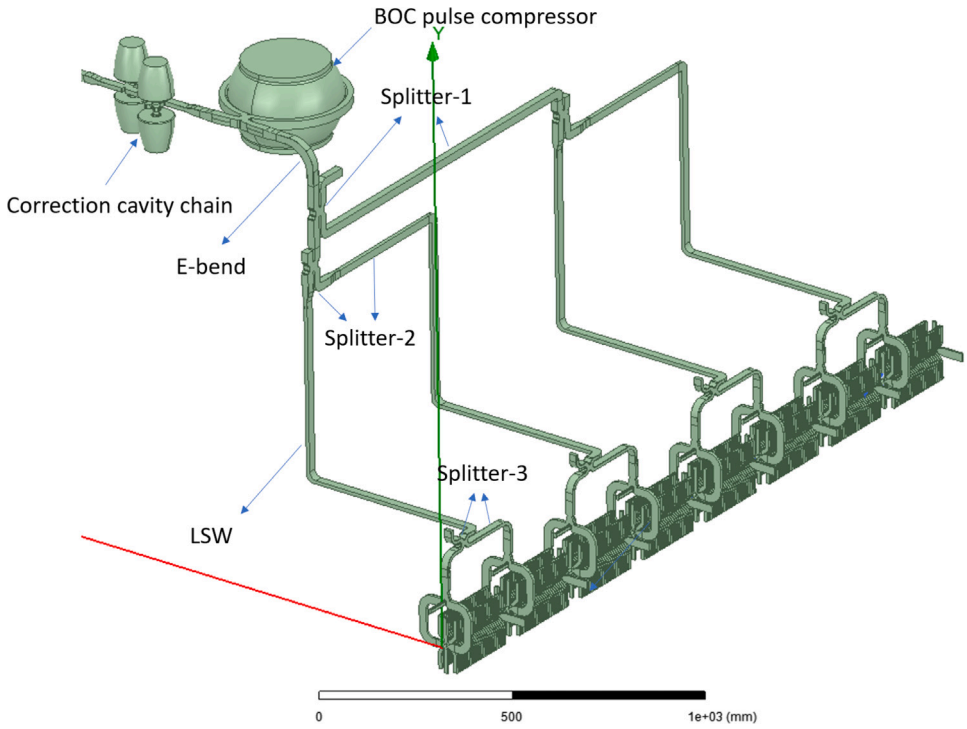

Fig. 18. RF design of the RF splitter based on LSW.

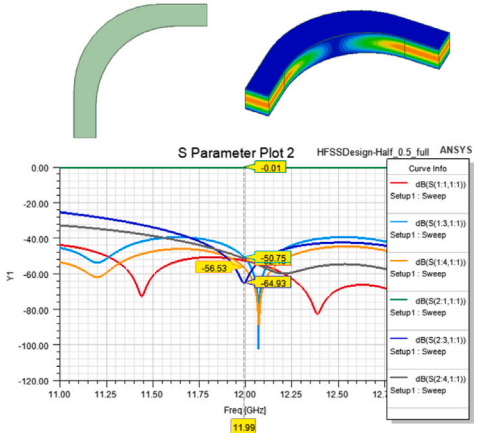

Fig. 19. RF design and S-parameters of the double-height E-bend.

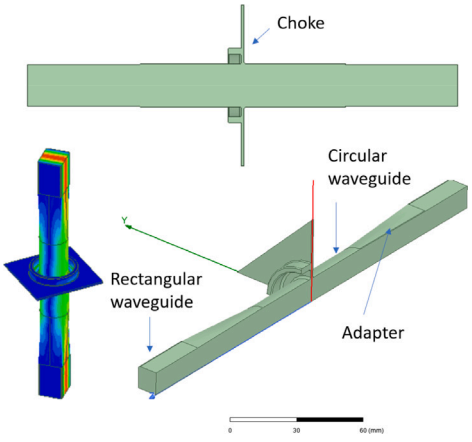

Fig. 20. RF design of the CMF.

Table 2
RF loss of the RF networks.

Components	RF loss (CMF)	RF loss (LSW)
Combiner	0.66%	0.66%
DHWG-90	4.01%	4.01%
CCC	1.29%	1.29%
BOC	2.01%	2.01%
H-bend	0.074%	0.0%
E-bend	0.28%	0.28%
CMF	0.29%	0.0%
E-bend	0.28%	0.0%
Splitter-1	0.98%	0.98%
Splitter-2	0.65%	0.85%
Splitter-3	0.62%	0.82%
LSW	0.0%	2.22%
Overall	10.66%	12.25%

were considered in these mechanical designs. Subsequently, detailed calculations and analyses of RF losses for the RF modules were conducted. Table 2 provides a summary of the calculated RF losses for the two RF networks for comparison. The overall RF losses amount to 10.66% and 12.25% for the CMF-based and LSW-based RF networks, respectively. Table 3 summarizes the surface electric field and modified poynting vector (S_c) of the two RF networks. The S_c is defined as $S_c = Re\{\bar{S}\}+1/6\cdot Im\{\bar{S}\}$, where $\bar{S}$ is the complex poynting vector [36]. The S_c is seen as a single RF breakdown constraint in RF design and used as a merit function when optimizing RF components in this paper. The pulse lengths are different for the RF power in Table 3. Before the BOC pulse compressor, the pulse length is 2500 ns and then the pulse length is about 330 ns as shown in Fig. 9.

7. Summary and conclusion

We present the RF module design based on double-height waveguides for the klystron-based CLIC, addressing two scenarios involving CMF and LSW for BBA. Comprehensive studies and designs for all RF components of the RF module consider factors such as compactness, reliability, and stability. Additionally, we offer an RF power loss

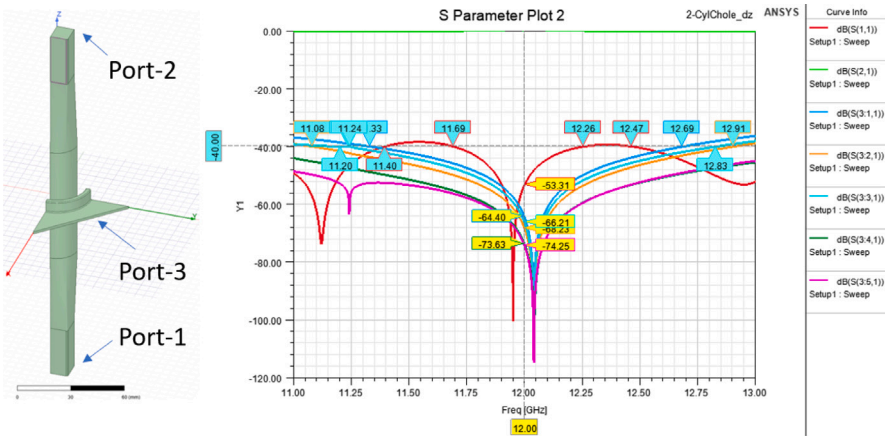

Fig. 21. S-parameters of the CMF in normal case.

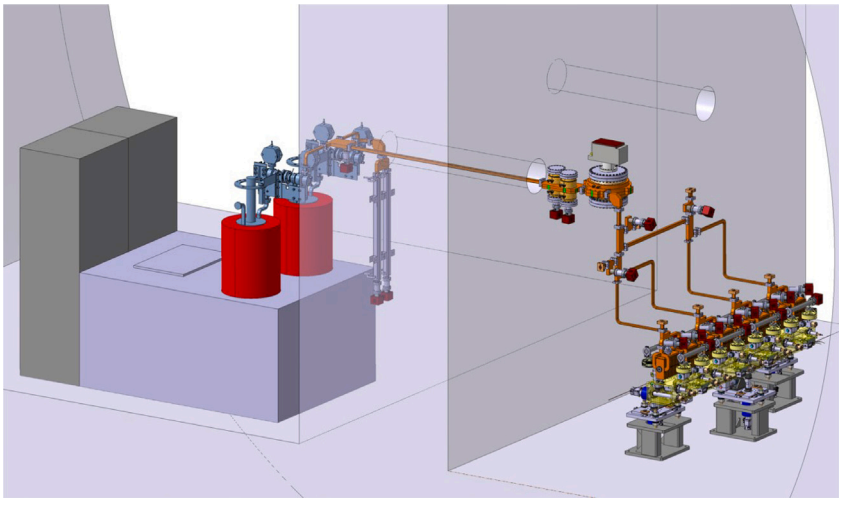

Fig. 22. Mechanical design of the RF module based on LSW.

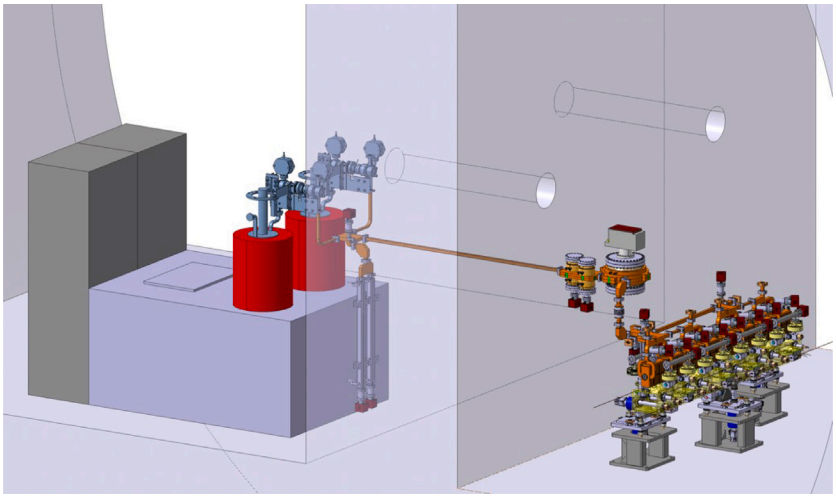

Fig. 23. Mechanical design of the RF module based on CMF.

Table 3
Surface fields of the RF networks.

Components	Emax [MV/m]	Sc [MW/mm^2]	Power [MW]
Combiner	25.9	0.55	100
DHWG-90	19.7	0.43	100
CCC	53.2	1.9	95
BOC	47.3	2.0	350
H-bend	45.9	2.0	350
E-bend	52.8	3.6	350
CMF	38.0	1.8	350
Splitter-1	48.4	1.9	350
Splitter-2	34.2	9.6	175

budget and maximum surface field values for each RF component. Wakefield simulations, varying settings for the input coupler, highlight the necessity of the HOMagic-T to damp the wakefields effectively. Two mechanical models, derived from RF designs of the RF module, have been thoroughly studied. The finalized RF design and mechanical design will be provided for the next stage, and prototypes of the RF components will under development and testing.

CRediT authorship contribution statement

P. Wang: Writing – original draft, Methodology, Investigation. **M. Capstick:** Visualization. **N. Catalan Lasheras:** Writing – review & editing, Resources. **S. Doebert:** Resources, Conceptualization. **A. Grudiev:** Writing – review & editing, Supervision, Conceptualization. **C. Rossi:** Resources, Conceptualization. **P. Morales Sanchez:** Visualization, Conceptualization. **I. Syratchev:** Methodology, Conceptualization. **X. Wu:** Investigation.

Declaration of competing interest

The authors declare that they have no known competing financial interests or personal relationships that could have appeared to influence the work reported in this paper.

Data availability

Data will be made available on request.

References

[1] M. Aicheler, P.N. Burrows, N. Catalan Lasheras, R. Corsini, M. Draper, J. Osborne, D. Schulte, S. Stapnes, M.J. Stuart, The Compact Linear Collider (CLIC) – Project implementation plan, in: M. Aicheler (Ed.), in: CERN Yellow Reports: Monographs, 2018, 247 p.

[2] M.J. Boland, et al., Updated baseline for a staged Compact Linear Collider, in: CERN Yellow Reports: Monographs, CERN, Geneva, 2016, Comments, 57 pages, 27 figures, 12 tables.

[3] M. Aicheler, P. Burrows, M. Draper, T. Garvey, P. Lebrun, K. Peach, N. Phinney, H. Schmickler, D. Schulte, N. Toge, A Multi-TeV Linear Collider Based on CLIC Technology: CLIC Conceptual Design Report, in: CERN Yellow Reports: Monographs, CERN, Geneva, 2012.

[4] L. Sánchez, D. Carrillo, D. Gavela, A. Lara, E. Rodríguez, J.L. Gutiérrez, J. Calero, F. Toral, A. Samoshkin, D. Gudkov, G. Riddone, Development and testing of a double length pets for the CLIC experimental area, Nucl. Instrum. Methods Phys. Res., A 746 (2014) 4–10.

[5] Günther Geschonke, A. Ghigo, CTF3 Design Report, Technical Report, CERN, Geneva, 2002, revised version number 1 submitted on 2002-06-19 12:11:29.

[6] Xian-Cai Lin, Hao Zha, Jia-Ru Shi, Liu-Yuan Zhou, Yi-Fan Liang, Jian Gao, Qiang Gao, Huai-Bi Chen, Chuan-Xiang Tang, Design, fabrication, and testing of low-group-velocity S-band traveling-wave accelerating structure, Nucl. Sci. Tech. 33 (11) (2022).

[7] Xian-Cai Lin, Hao Zha, Jia-Ru Shi, Qiang Gao, Jia-Yang Liu, Liu-Yuan Zhou, Jian Gao, Huai-Bi Chen, Chuan-Xiang Tang, Fabrication, tuning, and high-gradient testing of an X-band traveling-wave accelerating structure for VIGAS, Nucl. Sci. Tech. 33 (8) (2022).

[8] Jian Gao, Hao Zha, Jia-Ru Shi, Qiang Gao, Xian-Cai Lin, Fang-Jun Hu, Qing-Zhu Li, Huai-Bi Chen, Design, fabrication, and testing of an X-band 9 MeV standing-wave electron linear accelerator, Nucl. Sci. Tech. 34 (7) (2023).

[9] Mao-Mao Peng, Jia-Ru Shi, Hao Zha, Xian-Cai Lin, Ze-Ning Liu, Yu-Liang Jiang, Jian Gao, Liu-Yuan Zhou, Fo-Cheng Liu, Xiang-Cong Meng, Huai-Bi Chen, Development and high-gradient test of a two-half accelerator structure, Nucl. Sci. Tech. 32 (6) (2021).

[10] WenCheng Fang, DeChun Tong, Qiang Gu, ZhenTang Zhao, Design and experimental study of a C-band traveling-wave accelerating structure, Chin. Sci. Bull. 56 (2011) 18–23.

[11] A. Grudiev, W. Wuensch, Design of the CLIC Main Linac Accelerating Structure for CLIC Conceptual Design Report, 2010.

[12] Hao Zha, Andrea Latina, Alexej Grudiev, Giovanni De Michele, Anastasiya Solodko, Walter Wuensch, Daniel Schulte, Erik Adli, Nate Lipkowitz, Gerald S. Yocky, Beam-based measurements of long-range transverse wakefields in the compact linear collider main-linac accelerating structure, Phys. Rev. Accel. Beams 19 (2016) 011001.

[13] Hao Zha, Alexej Grudiev, Design and optimization of compact linear collider main Linac accelerating structure, Phys. Rev. Accel. Beams 19 (2016) 111003.

[14] Xiaoxia Huang, Alexej Grudiev, Zhentang Zhao, Wencheng Fang, CLIC380: RF design and parameters of 2017 re-baselined 380 GeV CLIC Linac accelerating structure, Nucl. Instrum. Methods Phys. Res. A 916 (2019) 230–237.

[15] William L. Millar, Alexej Grudiev, Walter Wuensch, Nuria Catalán Lasheras, Gerard McMonagle, Riccardo Zennaro, Paolo Craievich, Markus Bopp, Thomas G. Lucas, Matteo Volpi, Jan Paszkiewicz, Amelia Edwards, Rolf Wegner, Hikmet Bursali, Benjamin Woolley, Anastasiya Magazinik, Igor Syratchev, Anna Vnuchenko, Samantha Pitman, Verónica del Pozo Romano, David Ba nón Caballero, Graeme Burt, High-power test of two prototype X-Band accelerating structures based on SwissFEL fabrication technology, IEEE Trans. Nucl. Sci. 70 (1) (2023) 1–19.

[16] Xiaowei Wu, Jiaru Shi, Huaibi Chen, Jiahang Shao, Tetsuo Abe, Toshiyasu Higo, Shuji Matsumoto, Walter Wuensch, High-gradient breakdown studies of an X-band compact linear collider prototype structure, Phys. Rev. Accel. Beams 20 (2017) 052001.

[17] Jiayang Liu, Alexej Grudiev, RF Design of Accelerating Structure for the Main Linac of the Klystron-Based First Stage of CLIC at 380 Gev, Technical Report, CERN, Geneva, 2018.

[18] Zongbin Li, Wencheng Fang, Qiang Gu, Zhentang Zhao, RF design of a C-band compact spherical RF pulse compressor for SXFEL, Nucl. Instrum. Methods Phys. Res. A 863 (2017) 7–14.

[19] N. Shafqat, M. Trovo, I. Cudin, R. Fortunati, F. Gelmetti, L. Giannessi, T.G. Lucas, F. Marcellini, C. Masciovecchio, M. Milloch, A. Milocco, R. Zennaro, Fabrication, conditioning and installation of the 1st high gradient S-band accelerating module for the energy upgrade of the FERMI free electron laser Linac, Nucl. Instrum. Methods Phys. Res. A 1055 (2023) 168543.

[20] Urs Ellenberger, Heinrich Blumer, Markus Bopp, Alessandro Citterio, Mathias Heusser, Max Kleeb, Ludwig Paly, Markus Probst, Thomas Stapf, Riccardo Zennaro, The SwissFEL C-band RF pulse compressor: Manufacturing and proof of precision by RF measurements, in: Proceedings of the 36th International Free Electron Laser Conference, FEL 2014, Basel, Switzerland, 2014, pp. 25–29.

[21] Z.D. Farkas, H.A. Hogg, G.A. Loew, Pj B. Wilson, SLED: A method of doubling SLAC's energy, in: Proc. of 9th Int. Conf. on High Energy Accelerators, SLAC, 1974, p. 576.

[22] Youngdo Joo, Heung-Soo Lee, Woonha Hwang, Youngjung Park, Kyoungmin Oh, Byung-Joon Lee, Design study of a new SLED system with a biplanar 3-dB power divider and dual side-wall coupling-irises for the PAL XFEL, J. Korean Phys. Soc. 63 (2013) 1253–1261.

[23] Upgrades of S-band accelerating structures and pulse compressors in the electron and positron injector Linac of KEK, JACoW IPAC2023 (2023) WEPA118.

[24] Xiancai Lin, Hao Zha, Jiaru Shi, Yuliang Jiang, Fangjun Hu, Weihang Gu, Qiang Gao, Huaibi Chen, X-Band two-stage rf pulse compression system with correction cavity chain, Phys. Rev. Accel. Beams 25 (2022) 120401.

[25] Ping Wang, Hao Zha, Igor Syratchev, Jiaru Shi, Huaibi Chen, RF design of a pulse compressor with correction cavity chain for Klystron-based compact linear collider, Phys. Rev. Accel. Beams 20 (2017) 112001.

[26] Yuliang Jiang, Hao Zha, Ping Wang, Jiaru Shi, Huaibi Chen, William L. Millar, Igor Syratchev, Demonstration of a cavity-based pulse compression system for pulse shape correction, Phys. Rev. Accel. Beams 22 (2019) 082001.

[27] Jinchi Cai, Igor Syratchev, The Design Update of the X-Band RF Pulse Compressor with Correction Cavities for the CLIC 380 Gev Klystron Based Accelerator, Technical Report, CERN, Geneva, 2020.

[28] Xiaowei Wu, Alexej Grudiev, Novel open cavity design for rotating mode RF pulse compressors, Phys. Rev. Accel. Beams 24 (2021) 112001.

[29] P. Wang, A. Grudiev, RF design of the pulse compression system for the Klystron-based CLIC main Linac, in: JACoW IPAC, vol. 2023, 2023, p. WEPA115.

[30] Neven Blaskovic Kraljevic, Daniel Schulte, Beam-based beamline element alignment for the main Linac of the 380 GeV stage of CLIC, 2019, p. MOPMP018, http://dx.doi.org/10.18429/JACoW-IPAC2019-MOPMP018.

[31] Nuria Catalán Lasheras, Heiko Damerau, Romain Louis Gerard, Alexej Grudiev, Thomas Lucas, Gerard McMonagle, Jan Paszkiewicz, Sam Pitman, Anastasiya Solodko, Igor Syratchev, Anna Vnuchenko, Matteo Volpi, Benjamin Woolley, Walter Wuensch, Veronica del Pozo Romano, High power conditioning of X-Band RF components, 2018, p. WEPMF074, http://dx.doi.org/10.18429/JACoW-IPAC2018-WEPMF074.

[32] M. Boronat, N. Catalan-Lasheras, G. McMonagle, H. Bursali, A. Grudiev, I. Syratchev, High-power testing results of X-band RF window and 45 degrees spiral load, Power [MW] 35 (35) (2022) 35.
[33] D. Schulte, Multi-bunch calculations in the CLIC main LINAC, 2010.
[34] Alexej Grudiev, Design of Compact High Power RF Components at X-Band, Technical Report, CERN, Geneva, 2020.
[35] M. Capstick, S. Doebert, C. Rossi, J. Brown, Design, testing, and validating the CLIC module pre-alignment and alignment systems, JACoW IPAC 2023 (2023) MOPL101.
[36] A. Grudiev, S. Calatroni, W. Wuensch, New local field quantity describing the high gradient limit of accelerating structures, Phys. Rev. ST Accel. Beams 12 (2009) 102001.